Frontiers of Information Technology & Electronic Engineering
www.jzus.zju.edu.cn; engineering.cae.cn; www.springerlink.com
ISSN 2095-9184 (print); ISSN 2095-9230 (online)
E-mail: jzus@zju.edu.cn

Distributed multi-target tracking with labeled multi-Bernoulli filter considering efficient label matching#

Changwen DING[1], Chuntao SHAO[1], Siteng ZHOU[1], Di ZHOU[†‡1], Runle DU[2], Jiaqi LIU[2]

[1]*School of Astronautics, Harbin Institute of Technology, Harbin 150001, China*

[2]*National Key Laboratory of Science and Technology on Test Physics and Numerical Mathematics, Beijing 100076, China*

[†]E-mail: zhoud@hit.edu.cn

Received July 11, 2024; Revision accepted Oct. 25, 2024; Crosschecked Feb. 18, 2025; Published online Mar. 13, 2025

Abstract: We propose a distributed labeled multi-Bernoulli (LMB) filter based on an efficient label matching method. Conventional distributed LMB filter fusion has the premise that the labels among local densities have already been matched. However, considering that the label space of each local posterior is independent, such a premise is not practical in many applications. To achieve distributed fusion practically, we propose an efficient label matching method derived from the divergence of arithmetic average (AA) mechanism, and subsequently label-wise LMB filter fusion is performed according to the matching results. Compared with existing label matching methods, this proposed method shows higher performance, especially in low detection probability scenarios. Moreover, to guarantee the consistency and completeness of the fusion outcome, the overall fusion procedure is designed into the following four stages: pre-fusion, label determination, posterior complement, and uniqueness check. The performance of the proposed label matching distributed LMB filter fusion is demonstrated in a challenging nonlinear bearings-only multi-target tracking (MTT) scenario.

Key words: Distributed multi-sensor multi-target tracking; Labeled multi-Bernoulli filter; Arithmetic average fusion; Label matching

https://doi.org/10.1631/FITEE.2400582 **CLC number:** TP391

1 Introduction

Multi-target tracking (MTT) refers to jointly estimating the time-varying number and states of targets in noisy and cluttered tracking scenarios (Vo BN et al., 2014). However, even though MTT has a wide range of prospects in civilian and military applications (Hoseinnezhad et al., 2013; Katsilieris et al., 2015; Cai et al., 2019; Nguyen et al., 2021), it still faces numerous complex and intrinsic challenges due to the ubiquitous noisy measurements, missed detections, and unknown target-measurement matching.

As a promising approach first introduced by Mahler R (2007b), the random finite set (RFS) provides a unified framework for MTT and achieves mathematical consistency in Bayesian filtering algorithms. Tractable and approximate solutions have been proposed, including the probability hypothesis density (PHD) filter (Vo BN and Ma, 2006; Daniyan et al., 2017), the cardinalized probability hypothesis density (CPHD) filter (Mahler R, 2007a; Vo BT et al., 2007), the cardinality-balanced multi-target multi-Bernoulli (CBMeMBer) filter (Vo BT et al., 2009), and the Poisson multi-Bernoulli mixture (PMBM) filter (Garcia-Fernandez et al., 2018).

However, the RFS filters illustrated above are not real multi-target trackers since they just output

‡ Corresponding author

Electronic supplementary materials: The online version of this article (https://doi.org/10.1631/FITEE.2400582) contains supplementary materials, which are available to authorized users

ORCID: Changwen DING, https://orcid.org/0009-0007-2437-1833

target's estimated states, rather than the consecutive target trajectories. To overcome such deficiency, the labeled random finite set (LRFS) has been proposed (Vo BT and Vo, 2013), which allows target states to be augmented with corresponding identities. Based on LRFS, the generalized labeled multi-Bernoulli (GLMB) filter has been developed (Vo BT and Vo, 2013) which propagates GLMB densities according to the rigorous multi-target Bayesian recursion in a closed form. Considering the computational efficiency, the marginalized δ-GLMB (Mδ-GLMB) filter (Fantacci et al., 2016) and the labeled multi-Bernoulli (LMB) filter (Reuter et al., 2014) have been proposed. Moreover, to improve robustness and scalability, the distributed LRFS MTT has been widely studied.

The two most popular distributed fusion methods are log-linear generalized covariance intersection (GCI) and linear arithmetic average (AA). The weighted average Kullback–Leibler divergence (KLD) derived from local densities to fusion outcome can be minimized by the GCI fusion. A closed-form distributed GCI fusion of LRFS densities has been proposed based on the assumption that all local densities share the same labels (Fantacci et al., 2016). Relatively, the weighted average KLD derived from the fusion outcome to local densities can be minimized resorting to AA fusion, which guarantees the minimum information loss (MIL) (Gao et al., 2020b). AA fusion of PHD and multi-Bernoulli (MB) densities has been proposed by Li TC et al. (2020) and Li TC and Hlawatsch (2021). Considering its computational efficiency, AA fusion of PHD filters has been applied to distributed MTT in a sensor network with different fields of view (Li TC et al., 2019; Yi et al., 2020). For LRFS densities, AA fusion has been derived from MIL (Gao et al., 2020a). Moreover, a unified framework of AA fusion without statistical approximation has been proposed for the first time, which derives the proper AA fusion of different LRFS/RFS filters based on the unified LPHD/PHD-AA framework (Li TC, 2024).

Different from RFS, label matching shows paramount importance in the fusion of LRFS densities. Assuming that the identical label space is shared among sensor nodes and that the same label in different sensor nodes represents the same object, GCI fusion of LRFS densities has been developed (Fantacci et al., 2016). However, in practical tracking scenarios, sensor nodes are not necessarily sharing the identical label space, which is called label inconsistency. The fusion performance is highly affected by the label inconsistency, whose negative implications on LRFS densities have been analyzed theoretically (Li SQ et al., 2018). Since labels referring to different objects may be fused, this direct label-wise fusion of LRFS posteriors would give rise to a deteriorated result. To overcome such deficiency, a solution proposed by Li SQ et al. (2018) amounts to assigning labels to the unlabeled version of fused posteriors. Despite being able to guarantee the label consistency among different sensor nodes, this approach demands many computational resources.

A label matching GCI (LM-GCI) method, which minimizes the label inconsistency indicator derived from the GCI criterion, has been proposed by Li SQ et al. (2019). A lookup table to assign labels from different sensor nodes has been proposed by Shen et al. (2022). It has been proved that the LRFS density fusion can be resolved into two subproblems: label matching and density fusion (Gao et al., 2020a). Based on the label matching proposed by Li SQ et al. (2019), a slight improvement using Jensen–Shannon divergence (JSD) has been proposed to adapt to low detection probability scenarios (Gao et al., 2020a). The aforementioned label matching methods, however, rely on the matching cost function derived from the GCI fusion criterion. Due to the intrinsic multiplicative property of GCI fusion, it is essential to calculate the fractional power of the multi-object probability densities. This process suffers from higher computational complexity compared to the AA fusion. Furthermore, inheriting the limitations of GCI fusion, the accuracy of such label matching methods would significantly decrease when the sensor nodes are equipped with poor detection capability. Although an improvement has been proposed by Gao et al. (2020a), extra computational resources are still required.

In this paper, a distributed LMB filter based on efficient label matching is proposed. The main contributions are summarized as follows:

1. AA divergence is proposed from the perspective of AA fusion criterion, which reveals the discrepancy among local posteriors.

2. Considering different label matching, the proposed AA divergence is generalized to LRFS densities, and a label matching method for LMB densities

is derived. Compared with existing label matching methods, this proposed method shows higher performance in matching accuracy and computational efficiency, especially in low detection probability tracking scenarios.

3. To guarantee the consistency and completeness, the overall fusion procedure is designed into four stages, which not only achieves efficient label matching but also further ensures qualified fusion results.

2 Background

In this section, background knowledge of LRFS and distributed MTT is introduced, which is essential to this paper.

2.1 LRFS

An RFS is an element of $\mathcal{F}(\mathbb{X})$. $\mathcal{F}(\mathbb{X})$ represents all finite subsets of state space $\mathbb{X}$. It is worth noting that RFS is not in accordance with the Euclidian notion of integration and differential calculus. Accordingly, finite set statistics (FISST) supplies powerful and effective mathematical techniques to characterize RFS (Mahler RPS, 2003).

An RFS with distinct labels augmented to its state elements is called an LRFS X (Vo BT and Vo, 2013; Kropfreiter et al., 2020). Moreover, the labeled state space $\mathcal{X}$ is the product of the kinematic state space $\mathbb{X}$ and the discrete label space $\mathbb{L}$, i.e., $\mathbb{X}\times\mathbb{L}$. Let $f:\mathbb{X}\times\mathbb{L}\to\mathbb{R}$ be a function whose input is an LRFS and output is a real-valued number. Let $\mathcal{L}:\mathbb{X}\times\mathbb{L}\to\mathbb{L}$ denote the label projection, i.e., $\mathcal{L}((x,\ell))=\ell$. An MTT example resorting to LRFS is illustrated in Fig. 1, where not only target states but also different tracks have been extracted.

Hereafter, the standard inner product is represented as follows:

$$\langle h,k\rangle \triangleq \int h(x)\,k(x)\,\mathrm{d}x. \tag{1}$$

The exponential function of an RFS is represented as follows:

$$f^X \triangleq \prod\nolimits_{x\in X} f(x), \tag{2}$$

where $f:\mathbb{X}\to\mathbb{R}$, and $f^X=1$ when the set X is empty.

The definitions of the generalized Kronecker delta function $\delta_Y(X)$ and the generalized inclusion function $1_Y(X)$ can be found in Vo BT and Vo (2013). Moreover, the integration of function q defined on $\mathbb{X}\times\mathbb{L}$ is denoted as follows:

$$\int q(X)\,\delta X=\sum_{\ell\in\mathbb{L}}\int q(x,\ell)\,\mathrm{d}x. \tag{3}$$

For an LRFS, a tractable approximation was proposed by Papi et al. (2015). Considering an LRFS π on $\mathcal{F}(\mathbb{X}\times\mathbb{L})$ and $L_n=\{\ell_1,\ell_2,...,\ell_n\}$, the label set joint existence probability is represented as follows:

$$h(L_n)\triangleq\int\!\!\ldots\!\!\int\pi(\{(x_1,\ell_1),(x_2,\ell_2),...,(x_n,\ell_n)\})\mathrm{d}x_1\mathrm{d}x_2...\mathrm{d}x_n, \tag{4}$$

and the joint probability density function of states is represented as follows:

$$g\big(\{(x_1,\ell_1),(x_2,\ell_2),...,(x_n,\ell_n)\}\big)\triangleq\frac{\pi\Big(\Big\{(x_1,\ell_1),(x_2,\ell_2),...,(x_n,\ell_n)\Big\}\Big)}{h\Big(\Big\{\ell_1,\ell_2,...,\ell_n\Big\}\Big)}. \tag{5}$$

As a consequence, the density of an LRFS X_n can be generally described as the product of the joint existence probability and the joint probability density function as follows:

$$\pi\big(X_n\big)=h\big(L_n\big)g\big(X_n\big). \tag{6}$$

LMB is an important class of LRFS. For an LMB with parameter $\big\{\big(r^{(\ell)},p^{(\ell)}\big)\big\}_{\ell\in\mathbb{L}}$, the label set joint existence probability and the joint probability density function can be expressed as follows:

$$h(L_n)=\prod_{\ell\in\mathbb{L}}\Big(1-r^{(\ell)}\Big)\prod_{\ell'\in L_n}\frac{r^{(\ell')}}{1-r^{(\ell')}}, \tag{7}$$

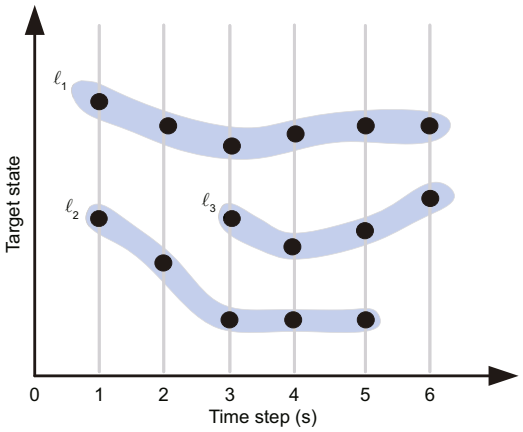

Fig. 1 A label assignment example for three different tracks where target states are represented by black dots and different tracks are represented by labels

$$g\left(X_n\right)=\prod_{\ell\in L_n}p^{(\ell)}(x), \tag{8}$$

where $r^{(\ell)}$ denotes the existence probability and $p^{(\ell)}=p^{(\ell)}(x)$ denotes the probability distribution.

2.2 LMB filter

LMB filter is established based on the multi-target Bayesian recursion (Fantacci et al., 2016). The label space is constructed in a recursive manner, which is represented as follows:

$$\mathbb{L}_{0:k}=\mathbb{L}_{0:k-1}\cup\mathbb{L}_{N(k)}, \tag{9}$$

where $\mathbb{L}_{0:k-1}$ represents the label space at time $k-1$ and $\mathbb{L}_{N(k)}$ represents the label space of newborn targets at time k. It is worth noting that $\mathbb{L}_{N(k)}$ and $\mathbb{L}_{0:k-1}$ are mutually exclusive.

The prediction step illustrates target dynamics, birth and disappearance. At time k, an LMB RFS modeling the birth targets is represented as follows:

$$\pi_{\mathrm{B}}=\left\{\left(r_{\mathrm{B}}^{(\ell)},p_{\mathrm{B}}^{(\ell)}\right)\right\}_{\ell\in\mathbb{L}_{N(k)}}. \tag{10}$$

At time k–1, the LMB posterior is represented as follows:

$$\pi_{k-1}=\left\{\left(r_{k-1}^{(\ell)},p_{k-1}^{(\ell)}\right)\right\}_{\ell\in\mathbb{L}_{0:k-1}}. \tag{11}$$

At time k, the predicted density is also an LMB, denoted as follows:

$$\begin{aligned}\pi_{k+}&=\left\{\left(r_{k+}^{(\ell)},p_{k+}^{(\ell)}\right)\right\}_{\ell\in\mathbb{L}_{0:k}}\\&=\left\{\left(r_{\mathrm{S},k+}^{(\ell)},p_{\mathrm{S},k+}^{(\ell)}\right)\right\}_{\ell\in\mathbb{L}_{0:k-1}}\\&\quad\cup\left\{\left(r_{\mathrm{B}}^{(\ell)},p_{\mathrm{B}}^{(\ell)}\right)\right\}_{\ell\in\mathbb{L}_{N(k)}},\end{aligned} \tag{12}$$

where

$$r_{\mathrm{S},k+}^{(\ell)}=h_{\mathrm{S}}(\ell)r_{k-1}^{(\ell)}, \tag{13}$$

$$p_{\mathrm{S},k+}^{(\ell)}=\frac{\left\langle p_{\mathrm{S}}\left(\cdot,\ell\right)f\left(x\mid\cdot,\ell\right),p_{k-1}\left(\cdot,\ell\right)\right\rangle}{h_{\mathrm{S}}\left(\ell\right)}, \tag{14}$$

$$h_{\mathrm{S}}\left(\ell\right)=\left\langle p_{\mathrm{S}}\left(\cdot,\ell\right),p_{k-1}\left(\cdot,\ell\right)\right\rangle, \tag{15}$$

$p_{\mathrm{S}}(\cdot,\ell)$ is the survival probability of the state, $f\left(x|\cdot,\ell\right)$ is the state transition function, and $h_{\mathrm{S}}\left(\ell\right)$ is the survival probability of track ℓ.

According to the multi-target Bayesian recursion, measurements are considered for the update step. The measurements are composed of target detections with noise and false alarms (clutter) illustrated by a Poisson RFS. Measurements can be generated with the detection probability $p_{\mathrm{D}}(x)$. The existence probability and probability density of track ℓ are given as follows:

$$r_k^{(\ell)}=\sum_{(I,\theta)\in\mathcal{F}(\mathbb{L})\times\Theta}\omega^{(I,\theta)}(Z)1_I\left(\ell\right), \tag{16}$$

$$p_k^{(\ell)}\left(x\right)=\frac{1}{r_k^{(\ell)}}\sum_{(I,\theta)\in\mathcal{F}(\mathbb{L})\times\Theta}\omega^{(I,\theta)}\left(Z\right)1_I\left(\ell\right)p^{(\theta)}\left(x,\ell\right), \tag{17}$$

where

$$\omega^{(I,\theta)}(Z)\propto\omega_{k+}^{(I)}\left[h_Z^{\theta}\right]^I, \tag{18}$$

$$p^{(\theta)}\left(x,\ell\right)=\frac{p_{k+}\left(x,\ell\right)\psi_z\left(x,\ell;\theta\right)}{h_z^{(\theta)}\left(\ell\right)}, \tag{19}$$

$$h_z^{(\theta)}\left(\ell\right)=\left\langle p_{k+}\left(\cdot,\ell\right),\psi_z\left(x,\ell;\theta\right)\right\rangle, \tag{20}$$

$$\begin{aligned}&\psi_z\left(x,\ell;\theta\right)\\&=\begin{cases}g\left(z_{\theta(\ell)}\mid x,\ell\right)p_{\mathrm{D}}\left(x\right)/k\left(z_{\theta(\ell)}\right), & \text{if }\theta(\ell)>0,\\1-p_{\mathrm{D}}\left(x\right), & \text{if }\theta(\ell)=0,\end{cases}\end{aligned} \tag{21}$$

Θ represents the space of mappings between measurements and tracks, and $\theta:I\to\{0,1,\ldots,|Z|\}$ is an element of Θ, such that $\theta\left(\ell\right)=\theta\left(\ell'\right)>0$ means $\ell=\ell'$. The pair $(I,\theta)\in\mathcal{F}\left(\mathbb{L}\right)\times\Theta$ denotes a potential hypothesis, the weight $\omega^{(I,\theta)}$ denotes this hypothesis probability, and $p^{(\theta)}\left(x,\ell\right)$ denotes the posterior when the track mapping is θ.

2.3 Distributed sensor network

The distributed sensor network illustrated in this paper is schematized in Fig. 2. Several sensor nodes, with capabilities of detection, computation, and communication, are dispersed in the network (Yang CQ et al., 2023). Resorting to the mathematical description of the graph, this network is modeled by $\mathcal{R}=(\mathcal{N},\mathcal{C})$, where $\mathcal{N}$ represents the sensor node set and $\mathcal{C}$ represents the set of communication routes, i.e., $\mathcal{C}\subseteq\mathcal{N}\times\mathcal{N}$. The number of sensor nodes is described as $|\mathcal{N}|$, and $\mathcal{N}^{(j)}\triangleq\{i:(i,j)\in\mathcal{C}\}$ denotes the nodes connected with node i (including node i itself) (Battistelli et al., 2013).

3 AA LMB fusion

In this section, we propose AA divergence and introduce AA LMB density fusion in MTT.

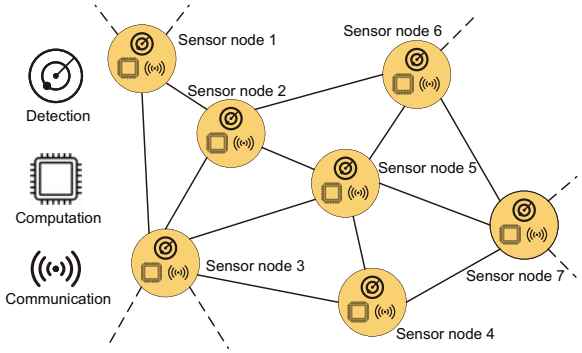

Fig. 2 Schematic of the sensor network

3.1 AA fusion and AA divergence

Local multi-target RFS probability densities with fusion weights can be represented as follows:

$$\Xi = \{(\pi_i(X), \omega_i)\}_{i\in\mathcal{N}}, \tag{22}$$

where $\omega_i > 0$ and $\sum_{i\in\mathcal{N}} \omega_i = 1$.

AA fusion can be obtained as the minimum of KLD average, which is given as follows:

$$\pi_{\mathrm{AA}} = \arg\min_{\pi} \sum_{i\in\mathcal{N}} \omega_i D_{\mathrm{KL}}(\pi_i \| \pi), \tag{23}$$

where $D_{\mathrm{KL}}(\cdot\|\cdot)$ represents the KLD between two probability densities.

Then, AA fusion is given as follows:

$$\pi_{\mathrm{AA}}(X) \triangleq \sum_{i\in\mathcal{N}} \omega_i \pi_i(X). \tag{24}$$

To measure the discrepancy among local multi-target densities, we introduce AA divergence to depict the information loss of AA fusion with local densities.

The MIL from an RFS density π to densities in Ξ is defined as follows (Gao et al., 2020a):

$$D_{\mathrm{MIL}}(\Xi \parallel \pi) \triangleq \sum_{i\in\mathcal{N}} \omega_i D_{\mathrm{KL}}(\pi_i \parallel \pi). \tag{25}$$

AA fusion minimizes the weighted average information loss according to Eq. (23), and the resulting minimal MIL is given as follows (Gao et al., 2020a; Yang F et al., 2022):

$$\min_{\pi} D_{\mathrm{MIL}}(\Xi \parallel \pi) = \sum_{i\in\mathcal{N}} \omega_i D_{\mathrm{KL}}(\pi_i \parallel \pi_{\mathrm{AA}}). \tag{26}$$

In this paper, we refer to the MIL given by Eq. (26) as AA divergence, denoted by $G(\Xi)$ as follows:

$$G(\Xi) = \sum_{i\in\mathcal{N}} \omega_i D_{\mathrm{KL}}\left(\pi_i \parallel \sum_{j\in\mathcal{N}} \omega_j \pi_j\right). \tag{27}$$

AA divergence can be measured to quantify the consistency among multiple densities. A minimal AA fusion divergence among densities in Ξ often indicates that the fusion adheres to the principle of minimum discrimination of information gracefully (Battistelli and Chisci, 2014), and therefore the fusion result guarantees a satisfactory consistency with respect to local densities.

Remark 1 Both AA and GCI fusions can deal with the double-counting phenomenon. Nevertheless, the product of local densities needs to be calculated in GCI fusion. When local densities are not qualified enough due to some sensor failures or low detection probabilities in the sensor network, the performance of GCI fusion degrades significantly. In particular, this may also be degenerated with the expansion of sensor networks. On the contrary, better tracking performance of AA fusion can be guaranteed under such circumstances.

3.2 AA fusion of LMB densities

Assuming that labels among sensor nodes have been matched, AA fusion of LMB densities has been achieved from two aspects (Gao et al., 2020a; Li TC, 2024). By restricting the form of the fusion outcome, a closed-form AA fusion result was derived (Gao et al., 2020a). Moreover, a unified framework of both RFS and LRFS density AA fusions was recently proposed based on PHD consistency (Li TC, 2024):

$$\overline{r}^{(\ell)} = \sum_{k\in\mathcal{N}} \omega_k r_k^{(\ell)}, \tag{28}$$

$$\overline{p}^{(\ell)} = \sum_{k\in\mathcal{N}} \hat{\omega}_k^{(\ell)} p_k^{(\ell)}, \tag{29}$$

where

$$\hat{\omega}_k^{(\ell)} = \frac{\omega_k r_k^{(\ell)}}{\sum_{i\in\mathcal{N}} \omega_i r_i^{(\ell)}}. \tag{30}$$

Remark 2 The prerequisite of the above LMB AA fusion is that labels among sensor nodes are exactly the same and have already been matched. As mentioned before, such prerequisite is impractical. Label matching will be investigated in Section 4.

4 AA fusion with efficient AA label matching

In Section 3, we have revealed AA fusion of LMB densities. However, as indicated in Eqs. (28) and

(29), this fusion procedure is label-wise. Considering that label inconsistency is ubiquitous and may degenerate the fusion results severely, therefore, label matching is a prerequisite for LMB fusion (Li SQ et al., 2018). In this section, we propose an AA fusion method with efficient label matching, which is based on the proposed AA divergence illustrated in Section 3.

4.1 Label matching description

Definition 1 Label matching is defined as a mapping function $\tau : \mathbb{L}_a \to \mathbb{L}_b$, where $\mathbb{L}_a$ is the label space of node a and $\mathbb{L}_b$ is the space of node b. The matching space is denoted as $\mathcal{T}(\mathbb{L}_a, \mathbb{L}_b)$. For any label ℓ of node a, i.e., $\ell \in \mathbb{L}_a$, $\tau(\ell)$ denotes the image of ℓ and $\tau(\ell) \in \mathbb{L}_b$.

Label matching τ connects potential identical targets between different sensor nodes. The subsequent fusion process will perform according to the matching results, and only correct matching is able to guarantee the qualified fusion estimates.

We assume one of the sensor nodes as the reference node, whose label space is denoted as $\mathbb{L}_{\text{ref}}$. $\tau_k : \mathbb{L}_k \to \mathbb{L}_{\text{ref}}$ represents a matching between labels of node k and the reference node, and $\tau_k(\ell) = \ell'$ denotes that labels ℓ and ℓ' are matched.

π_i is defined as the LRFS density of node i. Via label matching τ_i, its label space is matched with the reference node. Consequently, the global label matching of all sensor nodes is represented as follows:

$$\tau = \left(\tau_1, \tau_2, \ldots, \tau_{|\mathcal{N}|}\right). \tag{31}$$

For local LRFS densities $\Xi = \{(\pi_i(X), \omega_i)\}_{i\in\mathcal{N}}$, a generalized AA fusion with label matching can be expressed as follows:

$$(\pi_{\text{AA}}, \tau^*) = \arg\min_{(\pi,\tau)} \sum_{i\in\mathcal{N}} \omega_i D_{\text{KL}}^{(\tau_i)}(\pi_i \| \pi), \tag{32}$$

where $D_{\text{KL}}^{(\tau_i)}(\pi_i \| \pi)$ is the KLD of π_i and π when label matching is τ_i. τ^* is the optimal label matching.

Label matching is required for LRFS densities. As a result, it is introduced as an argument in the KLD of LRFS densities. Moreover, as illustrated in Gao et al. (2020a), label matching can be considered as an independent subproblem and is represented as an optimization of the generalized AA divergence:

$$\begin{aligned}\tau^* &= \arg\min_{\tau} G(\Xi) \\ &= \arg\min_{\tau} \sum_{i\in\mathcal{N}} \omega_i D_{\text{KL}}^{(\tau_i)}\left(\pi_i \| \sum_{j\in\mathcal{N}} \omega_j \pi_j\right).\end{aligned} \tag{33}$$

Remark 3 Eq. (33) is an optimization problem and can be illustrated as follows: cost is incurred when a sensor node's labels are matched with labels of other nodes. The purpose is to minimize the total cost by matching all labels of one node precisely with other nodes' labels.

4.2 Label matching for LMB densities

In the previous subsection, we have established the label matching problem and transformed it into an optimization issue. However, as multiple sensor nodes are considered, the optimization of Eq. (33) is a high-dimensional non-deterministic polynomial hard (NP-hard) puzzle, which is complicated to solve. We investigate an efficient solution to this problem.

To reduce the above optimization problem's dimension, the NP-hard problem can be simplified using a pair-wise realization (Li SQ et al., 2019). It can achieve a compromise between accuracy and computation efficiency, although it is suboptimal.

Without loss of generality, we take the LMB density fusion from sensor nodes a and b into consideration. The densities combined with fusion weights can be represented as $\{(\omega_a, \pi_a), (\omega_b, \pi_b)\}$. It can be readily extended to the fusion of more nodes by the pair-wise strategy.

Proposition 1 If π_a and π_b are two LMB densities parameterized by $\pi_a = \left\{\left(r_a^{(\ell)}, p_a^{(\ell)}\right)\right\}_{\ell\in\mathbb{L}_a}$ and $\pi_b = \left\{\left(r_b^{(\ell')}, p_b^{(\ell')}\right)\right\}_{\ell'\in\mathbb{L}_b}$, the cardinalities of $\mathbb{L}_a$ and $\mathbb{L}_b$ are identical, i.e., $|\mathbb{L}_a| = |\mathbb{L}_b|$, and the label matching between $\mathbb{L}_a$ and $\mathbb{L}_b$ is τ, then the matching cost function can be derived as follows:

$$J(\tau) = \sum_{\ell\in\mathbb{L}_a} G(\ell, \tau(\ell)), \tag{34}$$

where

$$\begin{aligned}&G(\ell, \tau(\ell)) \\ =&\omega_a\left(D_{\text{KL}}\left(r_a^{(\ell)} \parallel r^{(\ell)}\right) + r_a^{(\ell)} D_{\text{KL}}\left(p_a^{(\ell)} \parallel p^{(\ell)}\right)\right) \\ &+ \omega_b\left(D_{\text{KL}}\left(r_b^{(\tau(\ell))} \| r^{(\ell)}\right) + r_b^{(\tau(\ell))} D_{\text{KL}}\left(p_b^{(\tau(\ell))} \| p^{(\ell)}\right)\right),\end{aligned} \tag{35}$$

$$r^{(\ell)} = \omega_a r_a^{(\ell)} + \omega_b r_b^{(\tau(\ell))}, \tag{36}$$

$$p^{(\ell)} = \hat{\omega}_a^{(\ell)} p_a^{(\ell)} + \hat{\omega}_b^{(\tau(\ell))} p_b^{(\tau(\ell))}, \tag{37}$$

$$\hat{\omega}_a^{(\ell)} = \frac{\omega_a r_a^{(\ell)}}{\omega_a r_a^{(\ell)} + \omega_b r_b^{(\tau(\ell))}}, \tag{38}$$

$$\hat{\omega}_b^{(\tau(\ell))} = \frac{\omega_b r_b^{(\tau(\ell))}}{\omega_a r_a^{(\ell)} + \omega_b r_b^{(\tau(\ell))}}, \tag{39}$$

ω_a and ω_b are fusion weights, and $\sum_{i=a,b}\omega_i = 1$.

The proof of Proposition 1 is provided in the supplementary materials.

The following example illustrates the calculation of LMB AA divergence (matching cost) corresponding to different label matching solutions.

Example 1 Supposing that π_a and π_b are two LMB densities, both of which have two labeled Bernoulli components, the parameterized representations are $\pi_a = \left\{\left(r_a^{(\ell)}, p_a^{(\ell)}\right)\right\}_{\ell\in\mathbb{L}_a\subset\mathbb{L}}$, $\mathbb{L}_a = \left\{\ell_a^1, \ell_a^2\right\}$, $\pi_b = \left\{\left(r_b^{(\ell)}, p_b^{(\ell)}\right)\right\}_{\ell\in\mathbb{L}_b\subset\mathbb{L}}$, $\mathbb{L}_b = \left\{\ell_b^1, \ell_b^2\right\}$, where

$$r_a^{(\ell_a^1)} = 0.9, \quad p_a^{(\ell_a^1)} = \mathcal{N}\left(x; 100, 25\right),$$

$$r_a^{(\ell_a^2)} = 0.9, \quad p_a^{(\ell_a^2)} = \mathcal{N}\left(x; 60, 9\right),$$

$$r_b^{(\ell_b^1)} = 0.8, \quad p_b^{(\ell_b^1)} = \mathcal{N}\left(x; 102, 36\right),$$

$$r_b^{(\ell_b^2)} = 0.6, \quad p_b^{(\ell_b^2)} = \mathcal{N}\left(x; 58, 16\right).$$

Intuitively, ℓ_a^1 should be matched with ℓ_b^1, and ℓ_a^2 should be matched with ℓ_b^2. This will be further explained below by AA divergence.

Without loss of generality, π_a is selected as the reference density. There are two label matching solutions: τ_{I} and τ_{II}. τ_{I} is denoted as follows:

$$\tau_{\mathrm{I}} = \begin{cases} \ell_a^1 \leftrightarrow \ell_b^1, \\ \ell_a^2 \leftrightarrow \ell_b^2, \end{cases}$$

and τ_{II} is denoted as follows:

$$\tau_{\mathrm{II}} = \begin{cases} \ell_a^1 \leftrightarrow \ell_b^2, \\ \ell_a^2 \leftrightarrow \ell_b^1. \end{cases}$$

The local densities and different fusion results are illustrated in Fig. 3.

Resorting to Proposition 1, when label matching is τ_{I}, the AA divergence is 0.1407, and when label matching is τ_{II}, the AA divergence is 30.6786. It can be concluded that for LRFS densities, the AA divergence can be minimized when the optimal and reasonable label matching is adopted. Therefore, by minimizing the AA divergence of LRFS, the most reasonable label matching can be derived.

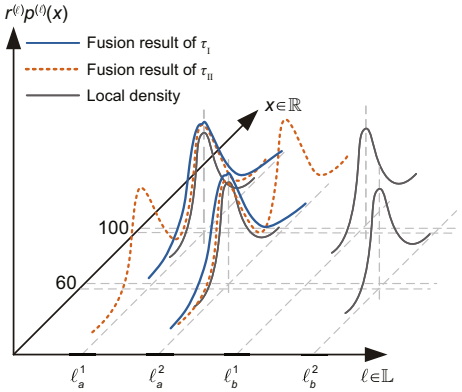

Fig. 3 Different label matching results

The cost of all label matching equals the sum of matching costs of each label in Proposition 1. Moreover, each label matching is irrelevant to the matching for other labels. Such a problem is illustrated as linear assignment. Based on these properties, the reasonable label matching solution and the minimum matching cost in Proposition 1 can be derived by using the Hungarian algorithm (Shopov and Markova, 2021) or the Jonker–Volgenant algorithm (Hamzehi et al., 2019) in polynomial computational complexity.

Remark 4 Note that the two LMB densities in Proposition 1 are defined in different label spaces, and the label matching is considered in the derivation of the cost function $J(\tau)$. For ease of derivation, the cardinalities of the two label spaces are assumed to be identical. Moreover, in Section 4.3, further research will be conducted when the cardinalities are different.

Remark 5 It can be seen that the KLD needs to be calculated in Eq. (35). The KLD for Gaussian distributions has an analytical expression. However, for Gaussian mixture (GM) models, KLD is not analytically tractable. Several efficient methods for approximating KLD between GMM have been proposed. We kindly ask readers to refer to Hershey and Olsen (2007) and Cui and Datcu (2015) for details.

Eventually, we denote "AA fusion" with the proposed efficient "AA label matching" as the AAF-AALM method. The procedure of AALM between sensor nodes a and b is illustrated in Algorithm 1.

Algorithm 1 AALM of LMB posteriors

Input: LMB posteriors parameterized by $\pi_a = \left\{\left(r_a^{(\ell)}, p_a^{(\ell)}\right)\right\}_{\ell\in\mathbb{L}_a}$, $\pi_b = \left\{\left(r_b^{(\ell')}, p_b^{(\ell')}\right)\right\}_{\ell'\in\mathbb{L}_b}$
Output: the optimal matching result τ^*, and the unmatched components π_a^{N}, π_b^{N}
Function AA_Label_Matching(π_a, π_b)
  $L_a = |\mathbb{L}_a|, L_b = |\mathbb{L}_b|, C_{\max}, \pi_a^{\mathrm{N}} = \varnothing, \pi_b^{\mathrm{N}} = \varnothing$
  Define an $L_a \times L_b$ cost matrix G
  for $\ell \in \mathbb{L}_a$ **do**
    for $\ell' \in \mathbb{L}_b$ **do**
      calculate the fused existence probability r: $r = \omega_a r_a^{(\ell)} + \omega_b r_b^{(\ell')}$
      $\tilde{\omega}_a^{(\ell)} = \omega_a r_a^{(\ell)}/r,\ \tilde{\omega}_b^{(\ell')} = \omega_b r_b^{(\ell')}/r$
      calculate the fused distribution p: $p = \tilde{\omega}_a^{(\ell)} p_a^{(\ell)} + \tilde{\omega}_b^{(\ell')} p_b^{(\ell')}$
      calculate $G(\ell, \ell')$ according to Eq. (35)
    end
  end
  $\tau^* = \text{optimal\_linear\_assignment}(G)$
  for $\ell \in \mathbb{L}_a$ **do**
    if $C(\ell, \tau(\ell)) > C_{\max}$
      $\pi_a^{\mathrm{N}} = \pi_a^{\mathrm{N}} \cup \pi_a^{(\ell)},\ \pi_b^{\mathrm{N}} = \pi_b^{\mathrm{N}} \cup \pi_b^{(\tau(\ell))}$
      remove matching $(\ell, \tau(\ell))$ from τ^*
    end
  end
  return τ^*, π_a^{N}, π_b^{N}

4.3 Fusion process with label matching

In the first two subsections, resorting to the proposed AA divergence, we have studied the implementation of converting the LMB label matching to a linear matching problem. In this subsection, further detailed fusion procedures with the proposed AA label matching method are illustrated.

To improve the computational efficiency, the local LMB posteriors can be pruned. The label matching threshold T is selected, and then only the Bernoulli component whose existence probability is greater than T will participate in the matching. We refer to these as "posteriors to be matched," denoted as $\pi_s^{\mathrm{M}}\ (s \in \mathcal{N})$:

$$\pi_s^{\mathrm{M}} = \left\{\left(r_s^{(\ell)}, p_s^{(\ell)}\right) : r_s^{(\ell)} > T\right\}_{\ell\in\mathbb{L}_s}, \tag{40}$$

$$\mathbb{L}_s^{\mathrm{M}} = \left\{\ell_s^i : r_s^i > T, s \in \mathcal{N}\right\}. \tag{41}$$

Accordingly, the "posteriors not to be matched" are denoted as $\pi_s^{\mathrm{NM}}\ (s \in \mathcal{N})$:

$$\pi_s^{\mathrm{NM}} = \pi_s \setminus \pi_s^{\mathrm{M}}, \tag{42}$$

$$\mathbb{L}_s^{\mathrm{NM}} = \mathbb{L}_s \setminus \mathbb{L}_s^{\mathrm{M}}. \tag{43}$$

For the sake of convenience, we consider sensors a and b as examples. It is worth noting that as described in Section 4.2, we can further extend the fusion process to more sensor nodes by using a pairwise realization method.

All the blue lines, depicted in Fig. 4, represent the optimal matching $\tilde{\tau}^*$ of labels to be matched in subspaces $\mathbb{L}_a^{\mathrm{M}}$ and $\mathbb{L}_b^{\mathrm{M}}$. It can be observed that the label indices corresponding to the subspaces $\mathbb{L}_a^{\mathrm{M}}$ and $\mathbb{L}_b^{\mathrm{M}}$ are not consistent with indices in the original spaces $\mathbb{L}_a$ and $\mathbb{L}_b$. Therefore, it is necessary to convert the optimal matching $\tilde{\tau}^*$, according to the classification result in Eqs. (40)–(43), back into the original spaces, i.e.,

$$\tilde{\tau}^* \to \tau^*, \tag{44}$$

where τ^* is the optimal matching in original spaces.

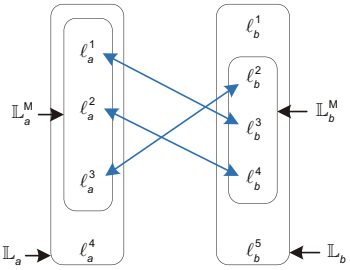

Fig. 4 A label matching example (References to color refer to the online version of this figure)

Furthermore, to preserve the integrality of the multi-target posterior, the labels not involved in matching are added to the final fusion result.

After matching the labels, fusion can be carried out according to AA fusion, as shown in Eqs. (28) and (29). In this paper, fusion is divided into the following four stages: pre-fusion, label determination, posterior complement, and uniqueness check.

In the pre-fusion stage, only the probability densities and the existence probabilities are fused according to the matching results. For instance, in GM implementation, the parameters of the fused probability density including the weight, mean, and covariance are determined at first. It is important to note that, to further improve the computational efficiency, at the end of this stage, pruning and merging of Gaussian components can be used.

In the label determination stage, since the Bernoulli components participating in matching

have their original labels, it is necessary to determine the finally fused posterior labels. In this stage, the fused label is determined by comparing the existence probabilities, which is given as follows:

$$\ell_{\mathrm{f}}^{i}=\begin{cases}\ell_{a}^{i}, & \text{if } \sum_{i=1}^{\left|\mathbb{L}_{a}^{\mathrm{M}}\right|} r_{a}^{i}>\sum_{i=1}^{\left|\mathbb{L}_{b}^{\mathrm{M}}\right|} r_{b}^{i},\\ \tau\left(\ell_{a}^{i}\right), & \text{otherwise,}\end{cases} \tag{45}$$

where ℓ_{f}^{i} denotes the fused label.

In the posterior complement stage, the labeled Bernoulli components in the local posterior that do not participate in label matching are augmented to the fusion result. For example, in Fig. 4, labels ℓ_a^4, ℓ_b^1, and ℓ_b^5 need to be appended into the fused posteriors.

Finally, the labels of the fused posterior obtained by the above procedures may be duplicated, so uniqueness check is required to ensure that the labels in the fusion posterior are unique.

The fusion procedures are illustrated in Algorithm 2.

Algorithm 2 AAF-AALM

Input: LMB posteriors parameterized by $\pi_a=\left\{\left(r_a^{(\ell)},p_a^{(\ell)}\right)\right\}_{\ell\in\mathbb{L}_a}$, $\pi_b=\left\{\left(r_b^{(\ell')},p_b^{(\ell')}\right)\right\}_{\ell'\in\mathbb{L}_b}$
Output: fused posterior π_{f}
Function AAF-AALM(π_a,π_b)
  classify π_a and π_b according to Eqs. (40)–(43) and obtain π_a^{M}, π_b^{M}, $\mathbb{L}_a^{\mathrm{M}}$, $\mathbb{L}_b^{\mathrm{M}}$, π_a^{NM}, π_b^{NM}
  $\tilde{\tau}^*,\ \pi_a^{\mathrm{N}},\ \pi_b^{\mathrm{N}}$ =AA_Label_Matching$\left(\pi_a^{\mathrm{M}},\pi_b^{\mathrm{M}}\right)$
  $\mathbb{L}_{\mathrm{f}}=\varnothing,\ \tilde{\mathbb{L}}_{\mathrm{f}}=\varnothing$
  convert label matching to original spaces: $\tilde{\tau}^*\to\tau^*$
  for $\ell\in\mathbb{L}_a^{\mathrm{M}}$ **do**
    // pre-fusion stage
    $\tilde{r}_{\mathrm{f}}^{(\ell)}=\omega_a r_a^{(\ell)}+\omega_b r_b^{(\tau^*(\ell))}$
    $\tilde{\omega}_a^{(\ell)}=\omega_a r_a^{(\ell)}/\tilde{r}_{\mathrm{f}}^{(\ell)},\ \tilde{\omega}_b^{(\tau^*(\ell))}=\omega_b r_b^{(\tau^*(\ell))}/\tilde{r}_{\mathrm{f}}^{(\ell)}$
    $\tilde{p}_{\mathrm{f}}^{(\ell)}=\tilde{\omega}_a^{(\ell)}p_a^{(\ell)}+\tilde{\omega}_b^{(\tau^*(\ell))}p_b^{(\tau^*(\ell))}$
    // label determination stage
    $\tilde{\ell}_{\mathrm{f}}^{(\ell)}=\begin{cases}\ell, & \text{if } \sum_{i=1}^{\left|\mathbb{L}_a^{\mathrm{M}}\right|} r_a^i>\sum_{i=1}^{\left|\mathbb{L}_b^{\mathrm{M}}\right|} r_b^i\\ \tau(\ell), & \text{otherwise}\end{cases}$
    $\tilde{\mathbb{L}}_{\mathrm{f}}=\tilde{\mathbb{L}}_{\mathrm{f}}\cup\{\tilde{\ell}_{\mathrm{f}}^{(\ell)}\}$
  end
  obtain $\tilde{\pi}_{\mathrm{f}}=\left\{\left(\tilde{r}_{\mathrm{f}}^{(\ell)},\tilde{p}_{\mathrm{f}}^{(\ell)}\right)\right\}_{\ell\in\tilde{\mathbb{L}}_{\mathrm{f}}}$
  // posterior complement stage
  $\tilde{\pi}_{\mathrm{f}}=\tilde{\pi}_{\mathrm{f}}\cup\pi_a^{\mathrm{NM}}\cup\pi_b^{\mathrm{NM}}\cup\pi_a^{\mathrm{N}}\cup\pi_b^{\mathrm{N}}$
  // uniqueness check stage
  for $i=1:|\tilde{\pi}_{\mathrm{f}}|$ **do**
    find repeated labels indexed as $\ell(i)$, denoted as label set rep$(\ell(i))$
    $r_{\mathrm{f}}(\ell(i))=\sum_{\ell\in\mathrm{rep}(\ell(i))}\tilde{r}_{\mathrm{f}}^{(\ell(i))}$
    $p_{\mathrm{f}}(\ell(i))=\bigcup_{\ell\in\mathrm{rep}(\ell(i))}\tilde{p}_{\mathrm{f}}^{(\ell(i))}$, $\mathbb{L}_{\mathrm{f}}=\mathbb{L}_{\mathrm{f}}\cup\{\ell(i)\}$
  end
  $\pi_{\mathrm{f}}=\left\{\left(r_{\mathrm{f}}^{(\ell)},p_{\mathrm{f}}^{(\ell)}\right)\right\}_{\ell\in\mathbb{L}_{\mathrm{f}}}$
  return π_{f}

5 Simulation results

This section carries out simulations to illustrate the performance of the proposed AAF-AALM. The GM model is used to represent the probability densities.

The state of the target is modeled as $x(t)=\left[p_x(t),e_x(t),p_y(t),e_y(t)\right]^{\mathrm{T}}$ at time t, where $\left[p_x(t),p_y(t)\right]^{\mathrm{T}}$ denotes the position and $\left[e_x(t),e_y(t)\right]^{\mathrm{T}}$ denotes the velocity in the two-dimensional coordinate system.

The dynamic model is illustrated by the nearly constant velocity (NCV) model, whose discretized form is described as follows:

$$x_{k+1}=Fx_k+G\eta_k, \tag{46}$$

where $F=\mathrm{diag}(F_1,F_1)$, $F_1=\begin{bmatrix}1 & T_{\mathrm{s}}\\ 0 & 1\end{bmatrix}$, $G=\mathrm{diag}(G_1,G_1)$, $G_1=\begin{bmatrix}T_{\mathrm{s}}^2/2\\ T_{\mathrm{s}}\end{bmatrix}$, $\eta_k=\begin{bmatrix}\eta_{x,k} & \eta_{y,k}\end{bmatrix}^{\mathrm{T}}$ is a discrete-time white process noise vector, and T_{s} represents the discrete time interval.

The process noise covariance in the discrete-time NCV dynamic model is as follows:

$$\mathrm{cov}(G\eta_k)=\mathrm{diag}\left(\mathrm{var}(\eta_{x,k})Q,\quad \mathrm{var}(\eta_{y,k})Q\right), \tag{47}$$

where

$$Q=\begin{bmatrix}T_{\mathrm{s}}^4/4 & T_{\mathrm{s}}^3/2\\ T_{\mathrm{s}}^3/2 & T_{\mathrm{s}}^2\end{bmatrix}. \tag{48}$$

Bearings-only measurements of targets are provided by each sensor. The measurement z_t^i at time t generated by the sensor node i is calculated as follows:

$$z_t^i=H^i(x_t)+v_t^i, \tag{49}$$

where v_t^i is a Gaussian distributed noise whose mean is zero and variance is $R^i=0.8^\circ$ and

$$H^i(x_t)=\mathrm{atan2}\left(p_x(t)-S_x^{(i)},p_y(t)-S_y^{(i)}\right), \tag{50}$$

atan2 represents the four-quadrant inverse tangent, and $\left(S_x^{(i)},S_y^{(i)}\right)$ denotes the coordinates of sensor node i.

The clutter is represented as a Poisson RFS, where the expected number is $\lambda_c = 6$ and the states are uniformly distributed across the observation area.

In this scenario, to evaluate the robustness and efficiency of AAF-AALM, the following three algorithms are used to demonstrate the performance:

(1) AAF-AALM, which is a combination of AA fusion with the proposed AA label matching method,

(2) AAF-GCILM, which is a combination of GCI-based label matching method proposed by Li SQ et al. (2019) and the AA fusion, and

(3) GCIF-GCILM, which is the GCI fusion combined with the GCI-based label matching method proposed by Li SQ et al. (2019). It is worth noting that GCIF-GCILM was called LM-GCI in Li SQ et al. (2019). In this paper, for the sake of comparison, we use GCIF-GCILM to represent LM-GCI.

In this scenario, the distributed sensor network consists of $|\mathcal{N}| = 7$ sensor nodes, which are dispersed at static prior known locations $\left(S_x^{(i)}, S_y^{(i)}\right)$ for each $i \in \mathcal{N}$. The positions of these seven sensors are listed in Table 1. Six targets are supposed to sequentially appear and then move within a two-dimensional 8000 m × 8000 m surveillance region. The scenario with real target trajectories and sensor positions is illustrated in Fig. 5.

Table 1 Positions of seven sensors in this scenario

Sensor	x (m)	y (m)
1	1600	7200
2	7200	6900
3	7500	1500
4	2000	100
5	2000	5000
6	6000	6000
7	2900	2000

For better comparison, both the distributed and centralized schemes are used in this scenario. In the distributed scheme, each sensor node can obtain the posterior of adjacent nodes and perform fusion (Battistelli et al., 2013; Šauša et al., 2024). Resorting to the consensus algorithm, all local fusion results tend to be consistent and optimal. In the centralized scheme, one of the nodes is regarded as the fusion center, receiving all the local posteriors and performing the fusion process. The suffix is appended to the algorithm to distinct the fusion

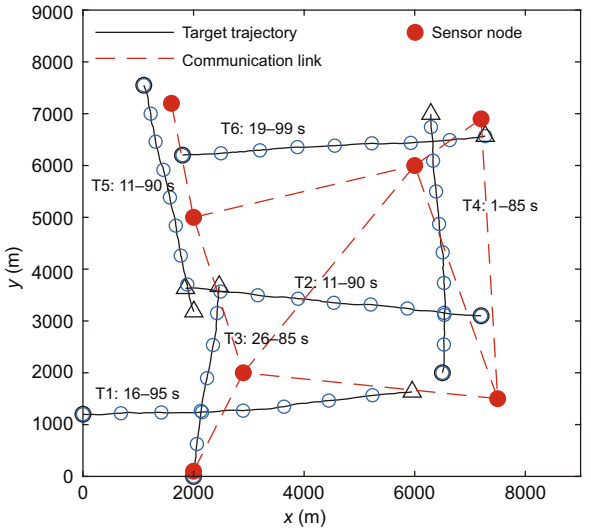

Fig. 5 A distributed network with seven bearings-only sensors and six targets, where black ∘ denotes the initial position, black △ denotes the end position, and blue ∘ denotes the position of the target every 10 s after birth. References to color refer to the online version of this figure

schemes. For instance, "AAF-AALM-K1" is the distributed AAF-AALM filter with only one consensus iteration. "AAF-AALM-Central" represents the centralized AAF-AALM filter.

The fusion weights of sensor nodes are determined as the metropolis weights (Fantacci et al., 2016), which are denoted as follows:

$$\omega^{(i,j)} = \begin{cases} \frac{1}{1+\max\left(|\mathcal{N}^{(i)}|,|\mathcal{N}^{(j)}|\right)}, i \in \mathcal{N}, j \in \mathcal{N}^{(i)} \setminus \{i\}, \\ 1 - \sum_{j \in \mathcal{N}^{(i)} \setminus \{i\}} \omega^{(i,j)}, i \in \mathcal{N}, j = i. \end{cases} \tag{51}$$

Relatively, in the centralized scheme, the fusion weights are identical, represented as follows:

$$\omega^{(i)} = \frac{1}{|\mathcal{N}|}, \ i \in \mathcal{N}. \tag{52}$$

Simulation results of one single run of AAF-AALM-K1 are shown in Fig. 6, and the detection probability is 0.9. It can be seen that all targets are assigned different labels and have been estimated successfully.

The average tracking performance of Optimal SubPattern Assignment (OSPA) errors (Schuhmacher et al., 2008) and cardinality distributions over 100 Monte Carlo simulations are illustrated in Figs. 7 and 8, respectively. We can see that AAF-AALM and AAF-GCILM provide similar tracking performances when the detection probabilities are

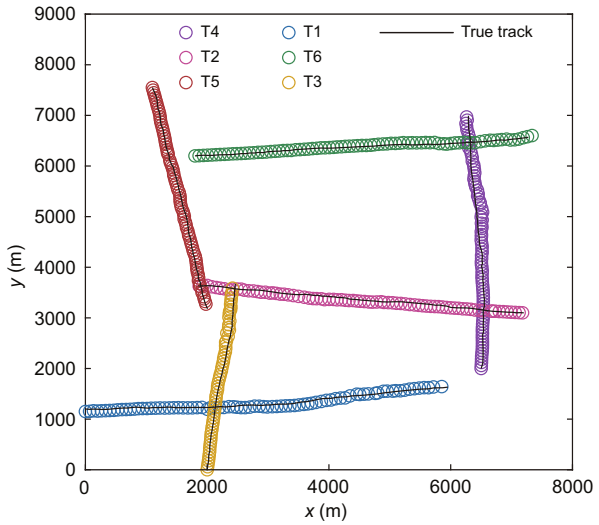

Fig. 6 Tracking results of AAF-AALM-K1 in one single run. References to color refer to the online version of this figure

0.99 and 0.80. However, when the detection probabilities are 0.50 and 0.30, compared to AAF-GCILM, AAF-AALM achieves a lower OSPA error. The density fusion methods adopted by AAF-AALM and AAF-GCILM are the same, and both of them are AA fusion. The only difference is the label matching method; one is AALM and the other is GCILM. So, it can be inferred that it is label matching that leads to the different final fusion results. Based on this, it can be concluded that compared to GCILM, AALM can still guarantee effective label matching under low detection probability scenarios.

Moreover, it has been shown that, compared to the other two methods, GCIF-GCILM achieves the worst results. As illustrated in Fig. 8, the cardinality estimate of GCIF-GCILM degrades severely as the detection probability decreases, which is consistent with the results derived in Gao et al.

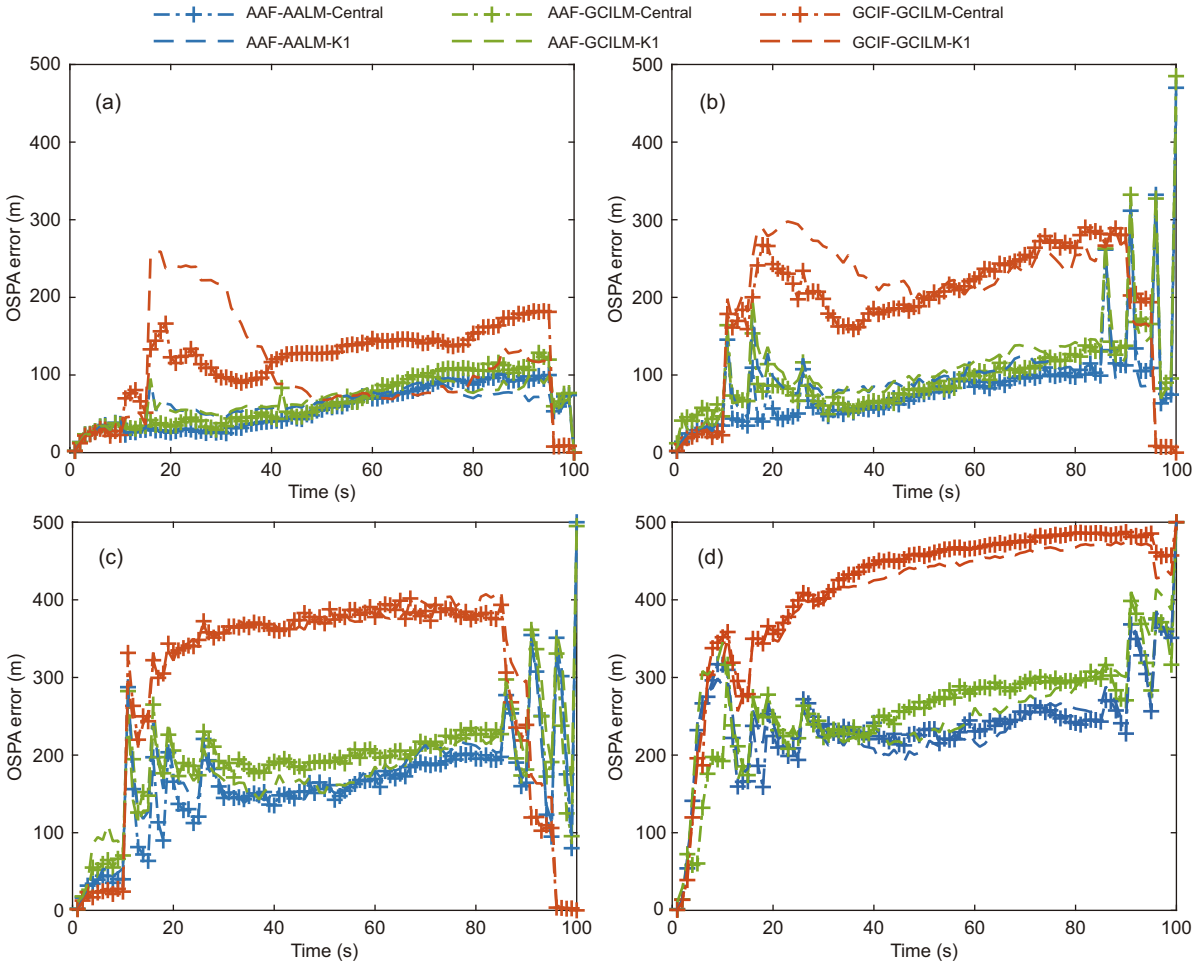

Fig. 7 OSPA errors under different detection probabilities: (a) 0.99; (b) 0.80; (c) 0.50; (d) 0.30

(2020a). However, as illustrated in Figs. 7 and 8, even in high detection probability scenarios, the performance of GCIF-GCILM is still worse than those of the other two AA fusion based methods. This is because only restricted information is provided in the bearings-only measurements, which leads to highly sensitive performance of GCI fusion once labels are mismatched. Furthermore, under low detection probability scenarios, AAF-AALM outperforms GCIF-GCILM distinctly, especially for cardinality estimation.

Under different detection probabilities, the average OSPA errors are illustrated in Fig. 9. It is shown that AAF-AALM achieves the best performance under the detection probability between 0.30 and 0.99. On the contrary, GCIF-GCILM has the worst performance in both distributed and centralized fusion schemes. Moreover, the OSPA error shows rapid growth when the detection probability is under 0.40.

To take into account track label errors (Vo BN et al., 2019), by using a suitable base distance, the OSPA$^{(2)}$ (OSPA-on-OSPA) metric addresses the above issue elegantly between two tracks (Beard et al., 2017). The OSPA$^{(2)}$ errors are illustrated in Fig. 10. All OSPA$^{(2)}$ errors increase as the detection probability decreases, but AAF-AALM achieves the smallest error in all detection cases, which resembles the performance in OSPA error.

To evaluate the performance of state localization estimation, the localization errors are shown in Fig. 11. It is worth pointing out that, when the detection probability is between 0.40 and 0.99, the localization error of GCIF-GCILM is lower than those of the other two AA fusion based methods. One reason why GCIF-GCILM has the

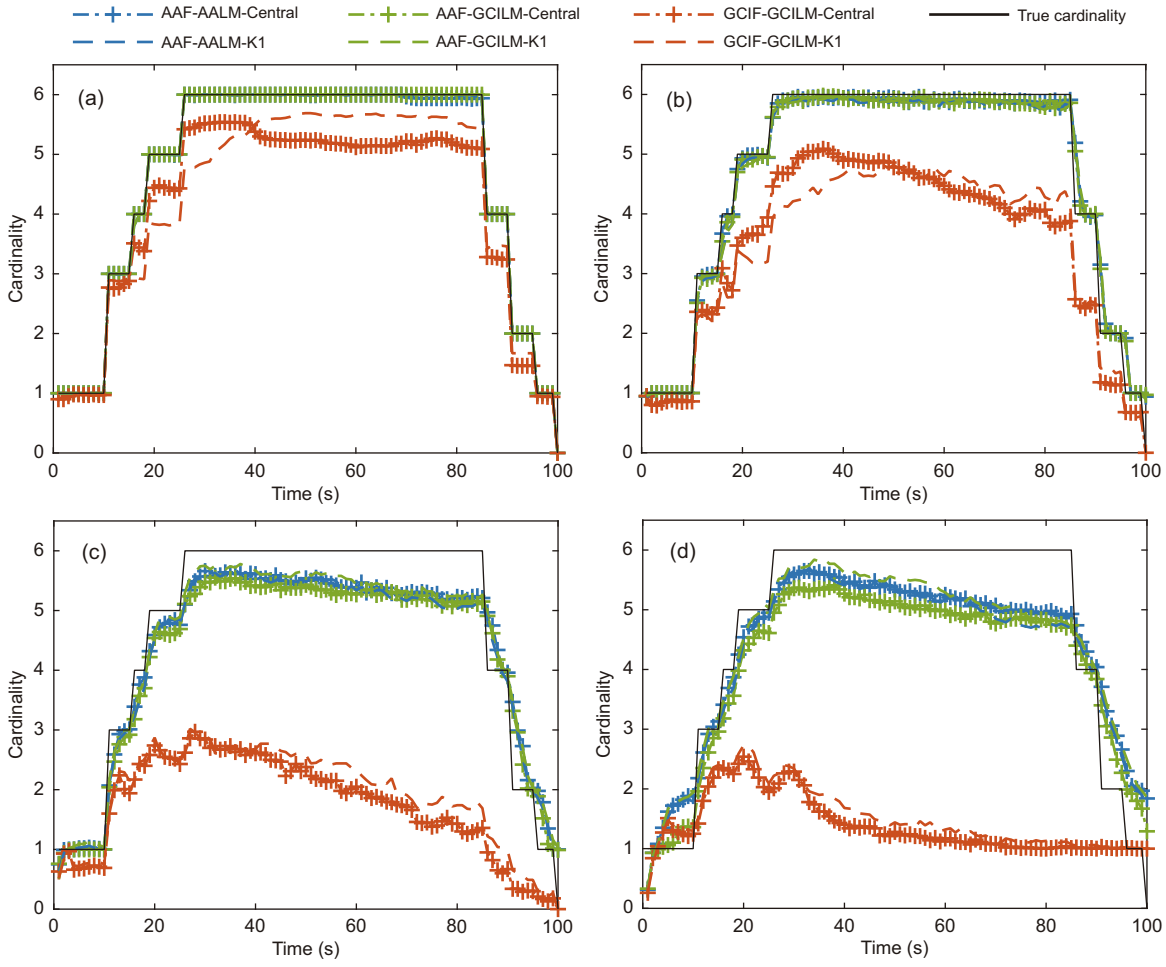

Fig. 8 Target cardinality under different detection probabilities: (a) 0.99; (b) 0.80; (c) 0.50; (d) 0.30

quite qualified performance in localization estimation whereas achieves the worst overall tracking result is that the GCI-based label matching method adopted in GCIF-GCILM cannot guarantee efficient matching, especially in low detection scenarios.

From the above results, it is shown that the proposed AAF-AALM outperforms AAF-GCILM in terms of state estimation, especially under low detection probabilities. Moreover, to further illustrate the performance in computation, the average execution time of AAF-AALM, AAF-GCILM, and GCIF-GCILM in the same complete MTT process is depicted in Fig. 12. It is shown that AAF-AALM exhibits much more computational efficiency compared to the other two methods, whereas AAF-GCILM suffers from the heaviest computational load. The main reason is that, in the GCI-based label matching method, the computational load increases distinctly with the increase in the number of potential targets, especially in the GM implementation, which requires complex exponentiation and integration of Gaussian probability density functions. However, in the AA-based label matching method, this kind of operation can be avoided, and thus the computational efficiency can be guaranteed. With the decrease of the detection probability, the execution time of AAF-GCILM and GCIF-GCILM increases obviously since when the detection probability decreases, the potential target number increases. On the contrary, the execution time of AAF-AALM remains steady with the variation of the detection probability, which reveals its robustness in computation.

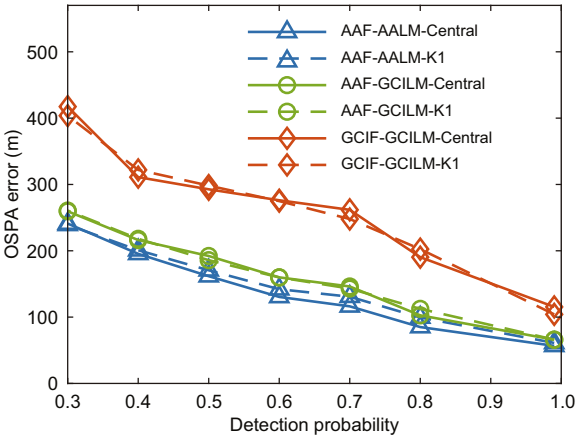

Fig. 9 OSPA errors under different detection probabilities

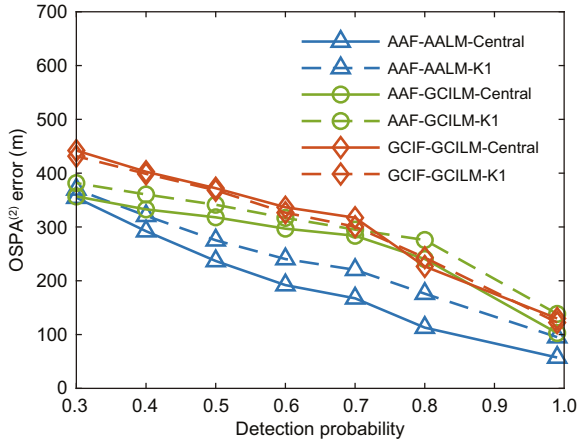

Fig. 10 OSPA$^{(2)}$ errors under different detection probabilities

6 Conclusions

A distributed LMB filter with efficient label matching has been proposed in this paper.

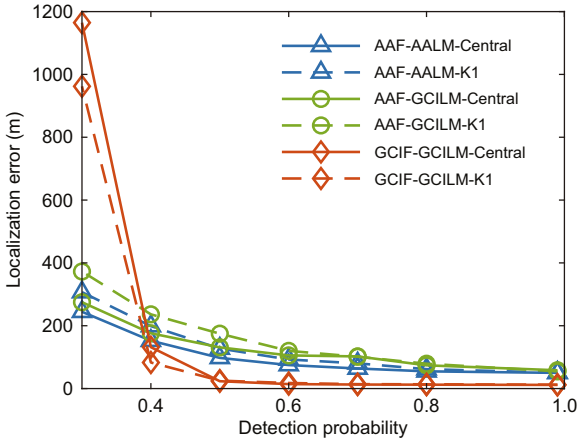

Fig. 11 Localization errors under different detection probabilities

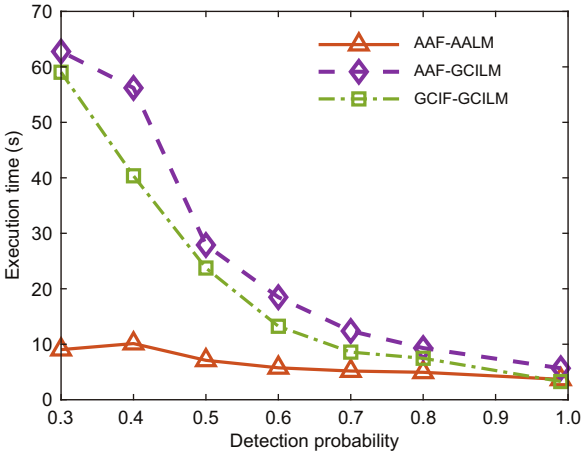

Fig. 12 Execution time under different detection probabilities

Considering the labels among local LMB densities that need to be consistent, this paper has proposed an efficient label matching method, called AALM. This AALM first establishes a cost function according to the proposed AA divergence, which evaluates the discrepancy among local posteriors from the perspective of AA mechanism, and then converts label matching into a linear assignment problem. The proposed label matching method is able to guarantee high performance even in low detection probability scenarios. Moreover, considering the practical problem of fusion implementation, four stages have been proposed in the fusion process, which are prefusion, label determination, posterior complement, and uniqueness check. The overall label matching LMB fusion process has been summarized, which guarantees the integrity and reliability of the fused posterior. Simulation results have demonstrated the effectiveness, efficiency, and robustness of the proposed algorithm in a distributed bearings-only MTT scenario.

Contributors

Changwen DING, Di ZHOU, and Runle DU designed the research. Changwen DING and Siteng ZHOU processed the data. Changwen DING drafted the paper. Chuntao SHAO, Runle DU, and Jiaqi LIU helped organize the paper. Changwen DING and Di ZHOU revised and finalized the paper.

Conflict of interest

All the authors declare that they have no conflict of interest.

Data availability

The data that support the findings of this study are available from the corresponding author upon reasonable request.

References

Battistelli G, Chisci L, 2014. Kullback–Leibler average, consensus on probability densities, and distributed state estimation with guaranteed stability. *Automatica*, 50(3):707-718. https://doi.org/10.1016/j.automatica.2013.11.042

Battistelli G, Chisci L, Fantacci C, et al., 2013. Consensus CPHD filter for distributed multitarget tracking. *IEEE J Sel Top Signal Process*, 7(3):508-520. https://doi.org/10.1109/JSTSP.2013.2250911

Beard M, Vo BT, Vo BN, 2017. OSPA$^{(2)}$: using the OSPA metric to evaluate multi-target tracking performance. Int Conf on Control, Automation and Information Sciences, p.86-91. https://doi.org/10.1109/ICCAIS.2017.8217598

Cai H, Gehly S, Yang Y, et al., 2019. Multisensor tasking using analytical Rényi divergence in labeled multi-Bernoulli filtering. *J Guid Contr Dynam*, 42(9):2078-2085. https://doi.org/10.2514/1.G004232

Cui SY, Datcu M, 2015. Comparison of Kullback-Leibler divergence approximation methods between Gaussian mixture models for satellite image retrieval. IEEE Int Geoscience and Remote Sensing Symp, p.3719-3722. https://doi.org/10.1109/IGARSS.2015.7326631

Daniyan A, Gong Y, Lambotharan S, et al., 2017. Kalman-gain aided particle PHD filter for multitarget tracking. *IEEE Trans Aerosp Electron Syst*, 53(5):2251-2265. https://doi.org/10.1109/TAES.2017.2690530

Fantacci C, Vo BN, Vo BT, et al., 2016. Consensus labeled random finite set filtering for distributed multi-object tracking. https://doi.org/10.48550/arXiv.1501.01579

Gao L, Battistelli G, Chisci L, 2020a. Fusion of labeled RFS densities with minimum information loss. *IEEE Trans Signal Process*, 68:5855-5868. https://doi.org/10.1109/TSP.2020.3028496

Gao L, Battistelli G, Chisci L, 2020b. Multiobject fusion with minimum information loss. *IEEE Signal Process Lett*, 27:201-205. https://doi.org/10.1109/LSP.2019.2963817

Garcia-Fernandez AF, Williams JL, Granstrom K, et al., 2018. Poisson multi-Bernoulli mixture filter: direct derivation and implementation. *IEEE Trans Aerosp Electron Syst*, 54(4):1883-1901. https://doi.org/10.1109/TAES.2018.2805153

Hamzehi S, Bogenberger K, Franeck P, et al., 2019. Combinatorial reinforcement learning of linear assignment problems. IEEE Intelligent Transportation Systems Conf, p.3314-3321. https://doi.org/10.1109/ITSC.2019.8916920

Hershey JR, Olsen PA, 2007. Approximating the Kullback Leibler divergence between Gaussian mixture models. IEEE Int Conf on Acoustics, Speech and Signal Processing, p.IV-317-IV-320. https://doi.org/10.1109/ICASSP.2007.366913

Hoseinnezhad R, Vo BN, Vo BT, 2013. Visual tracking in background subtracted image sequences via multi-Bernoulli filtering. *IEEE Trans Signal Process*, 61(2):392-397. https://doi.org/10.1109/TSP.2012.2222389

Katsilieris F, Driessen H, Yarovoy A, 2015. Threat-based sensor management for target tracking. *IEEE Trans Aerosp Electron Syst*, 51(4):2772-2785. https://doi.org/10.1109/TAES.2015.140052

Kropfreiter T, Meyer F, Hlawatsch F, 2020. A fast labeled multi-Bernoulli filter using belief propagation. *IEEE Trans Aerosp Electron Syst*, 56(3):2478-2488. https://doi.org/10.1109/TAES.2019.2941104

Li SQ, Yi W, Hoseinnezhad R, et al., 2018. Robust distributed fusion with labeled random finite sets. *IEEE Trans Signal Process*, 66(2):278-293. https://doi.org/10.1109/TSP.2017.2760286

Li SQ, Battistelli G, Chisci L, et al., 2019. Computationally efficient multi-agent multi-object tracking with labeled random finite sets. *IEEE Trans Signal Process*, 67(1):260-275. https://doi.org/10.1109/TSP.2018.2880704

Li TC, 2024. Arithmetic average density fusion—part II: unified derivation for unlabeled and labeled RFS fusion. *IEEE Trans Aerosp Electron Syst*, 60(3):3255-3268. https://doi.org/10.1109/TAES.2024.3359592

Li TC, Hlawatsch F, 2021. A distributed particle-PHD filter using arithmetic-average fusion of Gaussian mixture parameters. *Inform Fus*, 73:111-124. https://doi.org/10.1016/j.inffus.2021.02.020

Li TC, Elvira V, Fan HQ, et al., 2019. Local-diffusion-based distributed SMC-PHD filtering using sensors with limited sensing range. *IEEE Sens J*, 19(4):1580-1589. https://doi.org/10.1109/JSEN.2018.2882084

Li TC, Wang XX, Liang Y, et al., 2020. On arithmetic average fusion and its application for distributed multi-Bernoulli multitarget tracking. *IEEE Trans Signal Process*, 68:2883-2896. https://doi.org/10.1109/TSP.2020.2985643

Mahler R, 2007a. PHD filters of higher order in target number. *IEEE Trans Aerosp Electron Syst*, 43(4):1523-1543. https://doi.org/10.1109/TAES.2007.4441756

Mahler R, 2007b. Statistical Multisource-Multitarget Information Fusion. Artech House, Norwood, USA.

Mahler RPS, 2003. Multitarget Bayes filtering via first-order multitarget moments. *IEEE Trans Aerosp Electron Syst*, 39(4):1152-1178. https://doi.org/10.1109/TAES.2003.1261119

Nguyen TTD, Vo BN, Vo BT, et al., 2021. Tracking cells and their lineages via labeled random finite sets. *IEEE Trans Signal Process*, 69:5611-5626. https://doi.org/10.1109/TSP.2021.3111705

Papi F, Vo BN, Vo BT, et al., 2015. Generalized labeled multi-Bernoulli approximation of multi-object densities. *IEEE Trans Signal Process*, 63(20):5487-5497. https://doi.org/10.1109/TSP.2015.2454478

Reuter S, Vo BT, Vo BN, et al., 2014. The labeled multi-Bernoulli filter. *IEEE Trans Signal Process*, 62(12):3246-3260. https://doi.org/10.1109/TSP.2014.2323064

Šauša E, Rajmic P, Hlawatsch F, 2024. Distributed Bayesian target tracking with reduced communication: likelihood consensus 2.0. *Signal Process*, 215:109259. https://doi.org/10.1016/j.sigpro.2023.109259

Schuhmacher D, Vo BT, Vo BN, 2008. A consistent metric for performance evaluation of multi-object filters. *IEEE Trans Signal Process*, 56(8):3447-3457. https://doi.org/10.1109/TSP.2008.920469

Shen K, Dong P, Jing ZL, et al., 2022. Consensus-based labeled multi-Bernoulli filter for multitarget tracking in distributed sensor network. *IEEE Trans Cybern*, 52(12):12722-12733. https://doi.org/10.1109/TCYB.2021.3087521

Shopov VK, Markova VD, 2021. Application of Hungarian algorithm for assignment problem. Int Conf on Information Technologies, p.1-4. https://doi.org/10.1109/InfoTech52438.2021.9548600

Vo BN, Ma WK, 2006. The Gaussian mixture probability hypothesis density filter. *IEEE Trans Signal Process*, 54(11):4091-4104. https://doi.org/10.1109/TSP.2006.881190

Vo BN, Vo BT, Phung D, 2014. Labeled random finite sets and the Bayes multi-target tracking filter. *IEEE Trans Signal Process*, 62(24):6554-6567. https://doi.org/10.1109/TSP.2014.2364014

Vo BN, Vo BT, Beard M, 2019. Multi-sensor multi-object tracking with the generalized labeled multi-Bernoulli filter. *IEEE Trans Signal Process*, 67(23):5952-5967. https://doi.org/10.1109/TSP.2019.2946023

Vo BT, Vo BN, 2013. Labeled random finite sets and multi-object conjugate priors. *IEEE Trans Signal Process*, 61(13):3460-3475. https://doi.org/10.1109/TSP.2013.2259822

Vo BT, Vo BN, Cantoni A, 2007. Analytic implementations of the cardinalized probability hypothesis density filter. *IEEE Trans Signal Process*, 55(7):3553-3567. https://doi.org/10.1109/TSP.2007.894241

Vo BT, Vo BN, Cantoni A, 2009. The cardinality balanced multi-target multi-Bernoulli filter and its implementations. *IEEE Trans Signal Process*, 57(2):409-423. https://doi.org/10.1109/TSP.2008.2007924

Yang CQ, Cao XH, He LD, et al., 2023. Distributed multiple attacks detection via consensus AA-GMPHD filter. *IEEE Trans Syst Man Cybern Syst*, 53(12):7526-7536. https://doi.org/10.1109/TSMC.2023.3298646

Yang F, Zheng LT, Li TC, et al., 2022. A computationally efficient distributed Bayesian filter with random finite set observations. *Signal Process*, 194:108454. https://doi.org/10.1016/j.sigpro.2022.108454

Yi W, Li GC, Battistelli G, 2020. Distributed multi-sensor fusion of PHD filters with different sensor fields of view. *IEEE Trans Signal Process*, 68:5204-5218. https://doi.org/10.1109/TSP.2020.3021834

List of supplementary materials

Proof of Proposition 1